Inhibition of phosphodiesterase 10A by MP-10 rescues behavioral deficits and normalizes microglial morphology and synaptic pruning in a mouse model of FOXP1 syndrome

Henning Froehlich

henning.froehlich@med.uni-heidelberg.de

Heidelberg University

Jing Wang

University Hospital Heidelberg

Ferdinand Althammer

Heidelberg University

Tim Schubert

University Hospital Heidelberg

Nina Kluck

University Hospital Heidelberg

Valery Grinevich

Central Institute of Mental Health, University of Heidelberg https://orcid.org/0000-0002-6337-8866

Stefanie Schmitteckert

Christian Schaaf

Universitat Heidelberg, Germany

Gudrun Rappold

University Hospital Heidelberg https://orcid.org/0000-0002-3126-1508

Article

Keywords:

Posted Date: March 5th, 2024

DOI: https://doi.org/10.21203/rs.3.rs-3959100/v1

Additional Declarations: The authors have declared there is **NO** conflict of interest to disclose

Abstract

FOXP1 syndrome is caused by *FOXP1* haploinsufficiency and characterized by intellectual disability, speech and language impairment, autistic features and neuropsychiatric abnormalities such as anxiety and hyperactivity. Behavioral changes of respective patients are mirrored in *Foxp1*$^{+/-}$ mice. In this report, we demonstrate that decreased levels of Foxp1 in the *Foxp1*$^{+/-}$ striatum result in a significant decrease in phosphodiesterase 10a (Pde10a). Predominantly expressed in medium spiny neurons, Pde10a is involved in basal ganglia circuitry and cyclic nucleotide signalling. We also observed microglial activation and reduced synaptic pruning in the striatum of *Foxp1*$^{+/-}$ mice accompanied by an overexpression of inflammatory and microglia-associated genes (*Rhoa, Cd74*, *Ifi30* and *Fcgr2b*). This suggests that neuroinflammation contributes to the observed cognitive and behavioral deficits. Interestingly, treatment of *Foxp1*$^{+/-}$ mice with the specific PDE10A/Pde10a antagonist MP-10 (PF-2545920) immediately after birth not only corrected the behavioral abnormalities, including decreased ultrasonic vocalization, hyperactivity, and increased anxiety but also normalized the changes in microglial morphology and synaptic pruning. Since FOXP1 and its signaling pathway are highly conserved, we hypothesize that administration of MP-10 or other Pde10a antagonists may also alleviate the neurological dysfunction seen in humans with FOXP1 syndrome. We also discuss how altered FOXP1 expression may be responsible for the reduced PDE10A levels in Huntington's disease.

Introduction

Neurodevelopmental disorders affect around 15% of the population worldwide [1]. A key goal of research into neurodevelopmental disorders has always been to develop specific and effective therapies. Each genetically determined phenotype may, however, need to be treated and targeted differently, arguing for the development of stratified drugs for patients. As the etiology of many rare neurodevelopmental disorders is still poorly understood, this is a challenging task. According to Online Mendelian Inheritance in Man (OMIM) (https://www.omim.org/), more than 2800 cytogenic loci are currently associated with isolated intellectual disability (ID) or ID-associated disorders. A considerable number of the affected genes have been associated with autism spectrum disorders (ASD) and speech and language impairment, including forkhead box protein 1 FOXP1.

De novo haploinsufficiency of *FOXP1* results in a distinct syndrome (MIM 613670), characterized by mild to severe intellectual disability, speech and language impairment and behavioral abnormalities including autism spectrum disorder (ASD) or autistic features, repetitive behavior, anxiety, attention-deficit/hyperactivity and sensory symptoms [2–4]. Mitochondrial defects in the striatum and hippocampus contribute to the pathology [5, 6]. Other clinical findings may include refractive errors, strabismus, cardiac or renal abnormalities, cryptorchidism, hypertonia, hearing loss, epilepsy and gastrointestinal dysfunction in addition to the known neurological defects [3, 4, 7, 8]. However, despite exploring the pathogenesis of FOXP1 syndrome, effective treatments are still lacking. Therefore, this study investigates the possibility of treating FOXP1 syndrome.

FOXP1 belongs to the forkhead box P subfamily of genes, which consists of four members (FOXP1-4), three of which (FOXP1, FOXP2 and FOXP4) are expressed in the central nervous system [9,10]. It is highly conserved in vertebrates and expressed in the mouse in both the developing and adult brain, where it exhibits a specific abundance in the projection neurons of the striatum, the cortex (layer III to VIa), hippocampus (CA1 region), and thalamic nuclei [11–13]. The study of various mouse models has also shown that the striatum is particularly affected by Foxp1 deficiency [14–17]. In the striatum of embryonic and newborn Nestin-Cre (*Foxp1*$^{-/-}$) mice, which completely lack Foxp1 in the nervous system, the enzyme phosphodiesterase 10a (Pde10a) was one of 37 significantly dysregulated genes [7].

Because of its function and restricted expression, PDE10A has been considered a potential therapeutic target for various basal ganglia disorders [18–21]. We therefore hypothesized that dysregulation of PDE10A may also play a role in the pathology of FOXP1 syndrome. To test this, we analyzed *Foxp1*$^{+/-}$ mice, which best reflect human *FOXP1* haploinsufficiency. In stark contrast to Nestin-Cre (*Foxp1*$^{-/-}$) mice investigated earlier, which usually die two to three weeks after birth [16], *Foxp1*$^{+/-}$ animals do have a normal life expectancy and do not exhibit obvious changes in brain morphology. However, these animals display significant behavioral changes reminiscent of ASD, such as reduced neonatal ultrasonic vocalization (USV) and hyperactivity in the open field test [15].

In the current study, we investigated whether *Foxp1*$^{+/-}$ mice also show an altered Pde10a expression. We tested them for autism-like behavior, hyperactivity, anxiety and social behavior in the first 30 days after birth, as cognitive abnormalities manifest in individuals with FOXP1 syndrome in the first 3 years of age. In addition, we investigated to what extent continuous inhibition of Pde10a activity by the specific antagonist MP-10 (PF-2545920), an FDA-approved drug with a known safety profile, could correct the observed behavioral abnormalities in neonatal and juvenile *Foxp1*$^{+/-}$ animals.

Material and Methods

Animals

Mice were kept in a specific pathogen-free Biomedical Animal Facility under a 12-hour light/dark cycle with ad libitum access to water and food. All procedures were conducted in strict compliance with the National Institutes of Health Guidelines for the Care and Use of Laboratory Animals and approved by the National Institute of Mental Health animal care and use committee. The day of birth was considered as postnatal day (P) 0.5.

Generation of Nestin-Cre (Foxp1 $^{-/-}$) mice

Homozygous floxed *Foxp1* mice [22] were crossed with Nestin-Cre transgenic mice (B6.Cg-Tg(Nes-cre)1Kln/Jln) [23] heterozygous for the floxed *Foxp1* allele.

Generation of Foxp1$^{+/-}$ animals

WT female mice were crossed with male mice, heterozygous for the *Foxp1* KO allele (*Foxp1*$^{+/-}$) [24].

Floxed *Foxp1* mice, Nestin-Cre deleter mice and *Foxp1*$^{+/-}$ mice were backcrossed with C57BL/6J mice for at least 12 generations to obtain congenic animals.

Animal studies were approved by the Regierungspräsidium Karlsruhe, Germany (approval number 35-9185.81/G-105/16, 35-9185.81/G-86/14 and 35-9185.81/G-271/17).

Mouse treatment

A comparable number of male and female WT and *Foxp1*$^{+/-}$ mice received a daily dose of 1.5 mg/kg MP-10 (Merck KGaA, Darmstadt, Germany) (stock solution (20 mg/ml, dissolved in DMSO) diluted with PBS) or placebo by intraperitoneal injection starting immediately after birth, for a period of 29 consecutive days. To study microglia, animals were treated with the same dose of MP-10 from birth to P8.

cDNA synthesis

Total RNA was prepared from frozen mouse brain tissue samples using peqGOLD TriFast™ (PEQLAB-Life Science). First strand cDNA synthesis was performed with 1.5 µg RNA using a Superscript II reverse transcriptase kit (ThermoFisher Scientific) and oligo dT_{12-18}-primers (ThermoFisher Scientific) according to the manufacturer's instructions.

Quantitative real-time PCR

Quantitative real-time PCR was performed using the qTOWER system (Analytic Jena) with an annealing temperature of 60°C using SYBR Green No-ROX Fast Mix (Bioline) according to manufacturer's instructions. Each of the samples was analyzed in triplicate and relative mRNA levels were assessed using the Standard Curve Method by normalization to succinate dehydrogenase complex subunit A (*Sdha1*) and hypoxanthine phosphoribosyltransferase 1 (*Hprt1*). All primer sequences are listed in Suppl. Table 1.

nCounter analysis

Expression analysis was performed from 25 ng total RNA from striatal tissue using the nCounter system Gene 1 (NanoString Technologies, Seattle, WA, USA). The nCounter® Neuroinflammation Panel (XT-CSO-MNROI1-12) including site-specific markers was hybridized as recommended by the manufacturer. Background correction and normalization of data were performed via NanoStringsoftware nSolver 4.0 (NanoString Technologies). Stably expressed reference genes were chosen for normalization based on the geNorm method (see Suppl. Table 2).

Protein analysis

Protein isolation was performed using standard protocols. Western blot analysis was executed using the Odyssey Infrared Imaging System (LI-COR Biosciences, Lincoln, NE, USA). The following primary antibodies were used: rabbit anti Foxp1 (Abcam, Cambridge, UK), rabbit anti Pde10a (Abcam, Cambridge,

UK) and mouse anti GAPDH (Abcam, Cambridge, UK). IRDye 800CW and IRDye 680 (LI-COR Biosciences, Lincoln, NE, USA) were used as secondary antibodies according to manufacturer's instructions. Protein bands were quantified using Image Studio Lite 3.1 software (LI-COR Biosciences).

Behavioral testing

Pup ultrasonic vocalization (USV) recordings

Litters used for ultrasonic vocalization experiments had a maximum number of nine pups. At P3.5, animals were marked by foot tattoo with non-toxic animal tattoo ink. All measurements were performed in the light period at 22°C. P4.5, P7.5, and P12.5 pups were isolated from the mother and littermates in random order and placed in the open field (42 cm x 42 cm x 42 cm) for 5 min for USV recording, then immediately returned to the home cage. USV was recorded using an UltraSoundGate condenser microphone (CM16/CMPA, Avisoft Bioacoustics) placed 30 cm above the test arena. The microphones were connected to a computer via an Avisoft UltraSoundGate USG416H audio device. USV recordings were analyzed using SASLabPro software (Avisoft Bioacoustics) and a fast Fourier transform (FFT) was conducted (512 FFT length, 100% frame, Hamming window, 75%-time window overlap). To exclude software errors, the calls were also analyzed manually. The USV analysis was conducted in a blinded manner without knowledge of the genotype and sex of the pups.

Dark-light box

The two-compartment light-dark box test (also termed black-white box test or light–dark exploration test) is an ethological model of anxiety-like behavior designed for mice, based on the aversion of rodents to white and brightly illuminated compartments. The apparatus consists of a brightly lit (400 lx) larger chamber (41 cm x 41 cm) and a smaller dark chamber (20 cm x 41 cm). At P24 the mouse was placed into the dark chamber and automatically tracked and videotaped for 10 minutes (Sygnis-Tracker, Sygnis). Time spent in the light chamber, number of visits and total distance travelled was evaluated.

Hole board

At P26, the mice were placed in the centre of a Hole-Board (40 cm x 40 cm x 3.5 cm) containing 16 holes (diameter: 3 cm, depth: 3.5 cm). Animals were initially allowed to explore for 10 minutes. Head-dipping into the holes was automatically recorded via infrared emitters.

Elevated Plus Maze

The test measures the conflict between the natural tendency of mice to explore a novel environment and the aversive properties of a brightly lit open arena. The apparatus consists of a cross-shaped platform (gray, opaque plastic material, platform is 70 cm above the ground), with equally sized arms (W 6 cm × L 35 cm) and a central intersection (6 cm × 6 cm), allowing the animals to move freely into each zone of the maze. Two of the arms (opposite each other) are flanked by 17 cm opaque walls; the remaining two arms have no walls. Light intensities in the central zone, opened and closed arms were set to 230, 230 and 160 lux, respectively. Animals were placed in the central intersection and allowed to explore the maze

for 10 min. The experiment was monitored with a digital camera and Sygnis Tracker software. The number of visits, time and distance travelled in each arm were recorded. Visits of the open arm were calculated as percentage of total arm visits and time in the open arm was calculated as percentage of total arm time.

Social interaction

A social interaction box (Harvard Apparatus) divided into three compartments was used. The social arena consisted of a transparent box (42 × 60 cm) with two transparent sliding doors that divided the left, right, and center chambers (42 × 20 cm). In the first 5 min session, the tested mouse was placed in the central chamber with the sliding doors open to allow access to the other two chambers for habituation. In the second session, an empty cylindrical cage and another cylindrical cage housing an unfamiliar C57BL/6N mouse of the same sex and age as the tested mouse was placed in the corners of the left and right chambers. The tested mouse was placed in the central chamber and allowed to explore the arena for 5 min. Once this session was completed, another unfamiliar C57BL/6 mouse (novel mouse) with the same sex and age as the tested mouse was put in the empty cylindrical cage. The tested mouse was then allowed to explore the arena for 5 min. In the fourth session, the mouse in the cylindrical cage from session 2 was replaced by an unfamiliar C57BL/6 mouse of the opposite sex. The tested mouse was then allowed to explore the arena for 5 min. The location of the cages was rotated between trials. The number of observed contacts of the tested mice was counted manually.

Immunofluorescence

Mouse brains were fixed by perfusion with 4% paraformaldehyde and then dehydrated through an ethanol series and isopropanol. Brains were cleared in toluene prior to infiltration and embedded in paraffin for sectioning. 10 µm paraffin sections were prepared. Sections were deparaffinized and rehydrated through an ethanol series, followed by incubation in citrate buffer for antigen retrieval. Immunostaining was performed using standard protocols. Brain sections were incubated overnight with primary antibodies at 4°C and incubated with appropriate fluorescent secondary antibodies for 1hour at room temperature. The following primary antibodies were used: goat anti GFAP (Abcam, Cambridge, UK) 1:1000, rabbit anti Iba1 (ThermoFisher SCIENTIFIC, Dreieich, Germany) 1:1000.

Confocal microscopy and three-dimensional analysis of microglial morphology

For the three-dimensional reconstruction of microglia, z-stack images of the striatum (6–8 images per animal) were acquired (50 µm depth, 1 µm steps, × 40 magnification) using the Nikon AX confocal (Nikon Imaging Center, Heidelberg. Imaris (10.0, Oxford Instruments) was used to reconstruct and morphologically analyze microglia as previously described [25]. In brief, raw confocal files were imported into Imaris an further processed for surface reconstruction (background subtraction, surface detail 1.2µm, largest diameter 1.2 µm). Microglia with a volume < 150µm^3 or > 1500µm^3 were filtered out before data analysis. A new masked channel was created for filament analysis and we processed images using

automated threshold detection with maximum seed point placements. Starting points were added manually to ensure that each microglia had exactly one starting point in the soma center. For microglial morphology analysis, we calculated the average values for each animal individually (surface area, volume etc.) and data points reflect the mean values for each morphological parameter.

Sholl analysis was performed using Imaris in the filament reconstruction mode, and individual data sets were exported into separate Excel files for further analysis. In the respective sholl plots, each data point refers to the mean sholl intersections (average of the respective cohort, ±SEM, calculated from all microglia of each animal).

Data analysis and statistics

IBM SPSS STATISTICS 21 and Microsoft Office Excel software were used to analyze the data. Outliers in the data were determined via IBM SPSS STATISTICS 21 and excluded from further analysis. All data were checked for normal distribution via the Kolmogorov-Smirnov and Shapiro-Wilk test. If appropriate, two-way ANOVA was performed using litter as a cofactor.

Results

Foxp1 $^{+/-}$ striata exhibit reduced Pde10a mRNA and protein levels.

To investigate whether *Foxp1* haploinsufficiency leads to reduced Pde10a expression in striatal tissue as in the case of complete Foxp1 loss of Nestin-Cre (*Foxp1*$^{-/-}$) mice, we examined mRNA and protein expression of Pde10a at P1.5, P12.5 and in adult animals by quantitative real-time PCR and western blot, respectively. Both mRNA and protein levels were strongly reduced in *Foxp1*$^{+/-}$ striata. In P1 and P12, this reduction amounted to 32% and 40% at the mRNA level and 8% and 32% at the protein level. The strongest effect was observed in adults, where the reduction was 53% at the mRNA level and 51% at the protein level. (Fig. 1A). In the cortex, hippocampus and thalamus very low Pde10a expression was detected (Fig. 1B) and Pde10a mRNA levels were not significantly reduced in adult *Foxp1*$^{+/-}$ animals compared with wild type (WT) (Fig. 1C), indicating striatal specificity.

Long-term administration of MP-10 reverses behavioral deficits in juvenile Foxp1$^{+/-}$ animals

We next addressed the question whether inhibition of Pde10a in *Foxp1*$^{+/-}$ mice could alleviate the behavioral deficits that are associated with *FOXP1* haploinsufficiency. For treatment, we used one of the currently most advanced PDE10A inhibitors, the highly specific antagonist MP-10 (PF-2545920, Mardepodect). This drug exhibits an IC50 of 0.37 nM and > 1000-fold selectivity over other PDEs [26, 27] and has been shown to be safe and well tolerated at doses within the targeted efficacy range [28]. As reduced Foxp1 levels may already affect brain function at early postnatal stages, we started treatment of WT and *Foxp1*$^{+/-}$ mice immediately after birth (at P0.5) and continued administration of a daily dose of 1.5 mg/kg MP-10 or placebo for 29 consecutive days. The administered dose of MP-10 was well tolerated with no apparent side effects. During the treatment period, neonatal ultrasonic call behavior, anxiety and

hyperactivity were assessed (Fig. 2A). The behavior of treated WT mice did not differ from that of untreated WT mice, and no changes in body weight gain were observed during development. With exception of the elevated-plus-maze test (Fig. 2C) and social interaction test, which showed no differences between WT and *Foxp1*$^{+/-}$ animals, all other tests (neonatal ultrasonic vocalization, open field, hole board and dark-light-box) demonstrated significant behavioral alterations in *Foxp1*$^{+/-}$ mice compared with WT animals (Fig. 2B, D-F). All performed tests also showed significant behavioral changes between untreated and MP10-treated *Foxp1*$^{+/-}$ animals (Fig. 2B-F).

Since Nestin-Cre (*Foxp1*$^{-/-}$) mice show severely increased anxiety behavior (Suppl. Figure 1A-D) and anxiety disorders are common in people with FOXP1 syndrome, we performed several tests to investigate this further in *Foxp1*$^{+/-}$ animals. Here, we show that in the open field test *Foxp1*$^{+/-}$ mice traveled 117% more distance compared to WT littermates and covered 91% more distance in the corners, confirming the hyperactivity already described for this test [15]. In contrast, MP-10-treated *Foxp1*$^{+/-}$ animals did not differ from WT in their movement pattern (Fig. 2D). Neonatal ultrasonic calling was significantly reduced by approximately 27% in placebo-treated *Foxp1*$^{+/-}$ pups at P7.5 and P12.5. However, *Foxp1*$^{+/-}$ animals receiving MP-10 showed no difference in the number of calls compared with placebo-treated WT littermates (Fig. 2B). In the dark-light box test, both the number of visits to the light and the time spent in this compartment were significantly reduced by 57% and 73% respectively in *Foxp1*$^{+/-}$ mice compared to WT controls. In contrast, MP-10 treated *Foxp1*$^{+/-}$ animals did not show any behavioral changes and behaved like WT animals (Fig. 2E). The hole board test also showed aberrant behavior in *Foxp1*$^{+/-}$ animals with 45% less head dipping. MP-10-treated animals, on the other hand, did not differ from WT animals in this test (Fig. 2F).

In conclusion, all behavioral abnormalities analyzed in *Foxp1*$^{+/-}$ mice were significantly alleviated by the MP-10 treatment to the extent that they no longer differed from WT animals in the tests performed.

Foxp1 haploinsufficiency leads to striatal microglia activation and reduced microglia-mediated synapse elimination that is normalized by MP-10 treatment.

As there is increasing evidence that glial cell changes play a role in neurodevelopmental disorders such as ID and ASD [29–31], we examined both striatal astrocytes and microglia in WT and *Foxp1*$^{+/-}$ animals.

We compared microglia morphology by three-dimensional reconstruction at P8 in placebo- and MP-10-treated WT and *Foxp1*$^{+/-}$ pups in which treatment was started immediately after birth and continued daily as before. To this end, we labeled microglia by immunofluorescence antibody staining against ionized calcium-binding adaptor molecule 1 (Iba1) and analyzed microglial morphology and complexity using Imaris software. In total, we reconstructed and analyzed more than 65 000 microglia from 42 animals (n = 10/11) per group. As neuroinflammatory processes are characterized by a complex interplay between microglia and astrocytes, we also labeled the latter by immunofluorescence antibody staining of glial fibrillary acidic protein (GFAP) to assess the GFAP intensity as a potential readout of

astrogliosis/astrocyte hypertrophy in the *Foxp1*$^{+/-}$ striatum. No differences were detected between WT and *Foxp1*$^{+/-}$ astrocytes (Suppl. Figure 2A), and also the number of microglia did not differ between genotypes (Suppl. Figure 2B). But in contrast to astrocytes, *Foxp1*$^{+/-}$ microglia exhibited a 17% increase in cell volume and a 10% increase in area compared to WT microglia (Fig. 3A,B). In addition, filament length and branching were reduced by 19% and 25%, respectively (Fig. 3C,D,E), indicative of a pro-inflammatory microglial phenotype [25]. MP-10-treated *Foxp1*$^{+/-}$ animals, however, showed no difference in microglial cell volume, area, filament length, and branching compared with placebo-treated WT animals (Fig. 3A-F).

As microglia-mediated synaptic pruning has been considered as a critical step in refining the circuitry during development and disease, we examined synaptic pruning by determining the number of microglia-synapse contacts and the number of synapses engulfed by microglia. Synapses were marked by PSD-95 staining which labels postsynaptic density. Indeed, *Foxp1*$^{+/-}$ striata had 59% fewer contacts between microglia and synapses and the number of engulfed synapses was reduced by 59% (Fig. 4A-C). Remarkably, MP-10 administration also had a positive effect on microglial synapse contacts and engulfment, with MP-10-treated *Foxp1*$^{+/-}$ striata showing comparable numbers of contacts and engulfed synapses to WT tissue (Fig. 4A-C).

The changes in *Foxp1*$^{+/-}$ striatal microglia strongly suggest activation of microglia by neuroinflammatory processes. For this reason, bulk expression analysis of WT and *Foxp1*$^{+/-}$ striatal tissue at P8 was performed using a NanoString nCounter Neuroinflammation Panel of 770 target genes. A total of 64 genes showed nominally significantly altered expression in the *Foxp1*$^{+/-}$ striatum before correction for multiple testing (see Suppl. Table 2). Four genes (*Cd74*, *Ifi30*, *Fcgr2b* and *Rhoa*) were significantly upregulated in *Foxp1*$^{+/-}$ tissue by ≈ 163%, 55%, 54% and 10%, respectively (Fig. 5A,B). All four genes are associated with changes in microglial activity, as will be discussed below.

In conclusion, we found gene expression changes in the *Foxp1*-haploinsufficient striatum indicative of neuroinflammation, which is supported by altered microglial morphology and associated reduced microglial-mediated synapse elimination. In addition, we demonstrate that both microglial activation and altered synapse pruning can be prevented by early MP-10 treatment.

Discussion

Our study shows that reduced Foxp1 expression in the *Foxp1*$^{+/-}$ striatum is accompanied by greatly reduced Pde10a mRNA and protein levels during development and adulthood while the cortex, hippocampus, and thalamus are not affected. We can also demonstrate that continuous administration of the Pde10 antagonist MP-10 from birth can completely reverse early deficits in social behavior, anxiety disorders, and hyperactivity, as well as changes in striatal microglia and synaptic pruning.

It is well known that Pde10a modulates the signaling of the cyclic nucleotides cAMP and cGMP. Highly and almost exclusively expressed in striatal medium spiny neurons, it plays a critical role in regulating

striatal activity and basal ganglia circuitry [32, 33]. Blocking PDE10A with specific antagonists has previously reduced symptoms of Huntington's disease (HD) and Parkinsons's disease (PD) in mice, rats, and monkeys, although PDE10A expression is reduced in both disorders [34–36]. We now also show reduced Pde10a expression in *Foxp1*$^{+/-}$ animals. The reason why inhibition of this phosphodiesterase has a positive effect on symptoms can be explained by the fact that PDE10A antagonists act similarly to D2 receptor blockers by increasing the activity of D2-type medium spiny neurons (D2-MSNs) of the indirect (striatopallidal) pathway [37–40]. Due to a lower cAMP threshold in D1-type medium spiny neurons of the direct pathway (D1-MSNs) compared with D2-MSNs, antagonism of Pde10a may result in more pronounced downstream effects in D2-MSNs, ultimately leading to a balance between the direct and indirect pathways [39].

In this context, it is interesting to note that *Foxp1*$^{+/-}$ mice exhibit hyperexcitability of D2-MSNs, whereas no change was detectable in D1-MSNs [15, 41]. Increased intrinsic excitability, which was mainly due to downregulation of two classes of potassium currents (inward rectifying (K_{IR}) and leak currents (K_{Leak}) could also be confirmed in D2-MSNs with homozygous *Foxp1* deletion. The downregulation Kcnj2 and Kcnj4 for K_{IR} and Kcnk2 for K_{leak} detected in these neurons may underlie these currents [41]. As Pde10a is known to regulate intracellular signaling in striatal MSNs and exerts strong control over gene expression [42, 43], altered Pde10a expression may be responsible for the downregulation of these potassium channels.

We have demonstrated that *Foxp1*$^{+/-}$ mice exhibit alterations in striatal microglial morphology and reduced synaptic pruning in pups. Microglia, the resident immune cells of the central nervous system, constantly scan their local microenvironment and sense impairments triggered by endogenous and/or exogenous factors. In pathological conditions, microglia are activated and the resulting dysregulation of certain genes is thought to be an inevitable part of almost all CNS pathologies [44]. Reduced complexity and surface area in *Foxp1*$^{+/-}$ microglia indicate activation. Microglial activation is characterized by a transformation from a branched morphology with small cell bodies and highly branched, filamentous cell processes to a morphology with a large cell body and short, stout, unbranched cell processes, as has been described in early brain development [45]. The significantly increased expression of *Cd74*, *Rhoa*, *Ifi30* and *Fcgr2b* in the striatum of *Foxp1*$^{+/-}$ pups supports our findings. *Cd74* is strongly upregulated and considered a marker for reactive microglia, as it is more strongly expressed under disease conditions than in the healthy central nervous system [46, 47]. Moreover, it is well known that Cd74 mediates binding of the extracellular pro-inflammatory cytokine macrophage migration inhibitory factor, which is released in response to stress or an inflammatory response [48]. Rhoa is known to control reactivity and survival of microglia during neuroinflammation and there is new evidence of abnormal RhoA signaling in neurodegenerative diseases [49]. It is also assumed that altered Rhoa expression is involved in the pathogenesis of HD. Previous studies have shown increased mRNA levels of RhoA, ROCK and a number of downstream cytoskeleton-associated effector proteins in blood samples and in the frontal cortex of postmortem brain tissue from HD patients and in the striatum of the R6/2 HD mouse model [50]. The

strongest upregulation in our analysis has been detected for Fcgr2b. Increased expression of Fcgr2b appears to play a crucial role in PD, as it binds aggregated α-synuclein and thus inhibits phagocytosis of microglia through SHP-1 activation [51]. It is possible that this mechanism also contributes to the observed reduction of synaptic pruning in *Foxp1*$^{+/-}$ microglia. Ifi30 is known to play an important role in neurodegenerative processes.[52] Altered striatal microglial morphology and reduced synaptic pruning in *Foxp1*$^{+/-}$ pups could also be normalized by the treatment with MP-10. Our results thus confirm previous studies carried out in mouse models of PD that MP-10, like the Pde10A antagonist papaverine, has anti-inflammatory effects and inhibits both microglial activation and proinflammatory gene expression [18, 19].

There is already good evidence for a contribution of glial cells to the pathophysiology of ASD. Resting microglial cells are known to play an important role in regulating learning and memory, including modulation of memory strength, forgetfulness, and memory quality, through mediation of synaptic pruning. In response to neuroinflammation, microglia are activated and secrete proteins such as cytokines, chemokines, and reactive oxygen species. Through their dynamic morphological and functional properties, they influence synaptic function and plasticity [53]. Moreover, glial cell function is associated with an imbalance between excitatory and inhibitory synaptic functions [54, 55]. Indeed, brain samples from autistic individuals showed gliosis and increased glial proliferation [30], and animal models of ASD such as Rett syndrome, Fragile X syndrome, and a mouse model of tuberous sclerosis revealed glial abnormalities. Of note, we recently demonstrated mitochondrial dysfunction and increased oxidative stress in the *Foxp1*$^{+/-}$ striatum and hippocampus [5, 6]. Mitochondrial DNA is considered an important activator of inflammation and can lead to inflammasome activation when it escapes from stressed mitochondria [56, 57]. For this reason, it is likely that mitochondrial dysfunction in the *Foxp1*$^{+/-}$ brain contributes to or is even causative for the development of the observed microglial abnormalities. Further studies should clarify whether the improvements in behavior after MP-10 administration are due to an effect of the compound on mitochondrial function and accumulation of ROS in MSNs and possibly microglia.

Alterations in cortical-subcortical circuits have been shown to affect motor function, cognition, and emotional behavior. It is evident today that neurodegenerative diseases such as HD and PD, as well as psychiatric disorders such as schizophrenia (SCZ) and profound developmental disorders such as ASD and anxiety disorders, all have dysfunction of the corticostriatal circuits and imbalances of the direct and indirect basal ganglia pathways as their neurobiological basis [58–60]. Moreover, it is well established that movement disorders and altered basal ganglia circuits in HD, PD, and SCZ are associated with changes in PDE10A expression and function [21]. In addition, mutations in *PDE10A* itself cause childhood-onset chorea with striatal lesions [61]. Therefore, this molecule is considered a potential therapeutic target for these aforementioned disorders as well as other basal ganglia disorders [21, 62–66]. Indeed, autism-like behaviors induced in rats by administration of valproic acid or a serotonin receptor agonist were significantly attenuated by treatment with papaverine, a PDE10A antagonist.[65] Furthermore, the treatment had a positive effect on neuroinflammatory processes and oxidative stress. However, compared to MP-10,

a potent, orally active and selective PDE10A inhibitor with an IC50 of 0.37 nM, with > 1000-fold selectivity over other PDEs, papaverine has significantly lower potency and selectivity and a very short exposure half-life after systemic administration.[27]

With regard to HD, it is interesting to note that both HD mouse models and HD patients have reduced levels of PDE10A as well as reduced levels of FOXP1 [67–69]. Based also on the fact that Pde10a is a Foxp1 target and is decreased in both Nestin-Cre (*Foxp1*$^{-/-}$) and *Foxp1*$^{+/-}$ mice, it is reasonable to assume that reduced Foxp1 expression may also be responsible for the reduced striatal Pde10a levels in HD. Phase II clinical trials with MP-10 (NCT01806896, NCT02197130, NCT02342548) in patients with full-blown symptoms of HD, however, failed to meet the pre-specified endpoints of the trial, despite the promising data in HD mouse models [35, 36]. However, this result cannot be extrapolated to FOXP1 syndrome as explained below. First, the timepoint of therapeutic intervention may be crucial for success. It is increasingly understood that therapeutic interventions during sensitive periods in brain development, typically before the onset of symptoms, will affect prospective results. Altered PDE10A expression has already been described well before the symptomatic onset in HD [70], which renders it likely that at the clinical onset, most of the neurons are already affected. This might flag them for destruction, so that dysregulated PDE10A-mediated intracellular signaling may represent an early phenomenon in this late-onset disorder. Second, in cortical neurons expressing mutant htt, elevated Foxp1 expression protected these cells from cell death [67], whereas knockdown of Foxp1 in healthy neurons promoted cell death [67]. These findings convincingly show that FOXP1 plays a neuroprotective role in striatal and cortical neurons and that reduced FOXP1 expression causes the selective neurodegeneration of striatal and cortical neurons in HD brains [67]. But apart from enlarged lateral ventricles in some individuals with FOXP1 syndrome, there are no obvious signs of striatal neurodegeneration in either humans or mice with loss of a *FOXP1* allele [71, 72]. *Foxp1*$^{+/-}$ animals exhibit a decrease in *Foxp1* mRNA and protein of ≈ 41% and ≈ 52%, respectively, at P1, P12, and adulthood compared with WT animals [5]. Significantly lower FOXP1 levels were also observed in both a HD mouse model and HD patients [70]. Therefore, it is reasonable to assume that FOXP1 levels in HD patients gradually decrease with age.

To date, more than 200 individuals with a pathogenic variant in FOXP1 have been documented, but this number is expected to increase due to genetic testing. As the FOXP1 transcription factor and its regulatory networks are highly conserved [73] it is likely that reduced PDE10A expression is a major contributor to the symptomatology not only in mice but also in humans with FOXP1 syndrome. As the 4-week treatment period in newborn mice is equivalent to more than a decade of life in children, further studies can now be carried out to find out whether the start of treatment also at later developmental time points is beneficial and whether inhibition of Pde10a by MP-10 also ameliorates learning and memory deficits during later development.

Most of the individuals affected with FOXP1 syndrome exhibit autistic traits. In addition, there are behavioral problems such as hyperactivity, attention problems, impulsivity, aggression, anxiety, mood instability, obsessions and compulsions. Moreover, many suffer from attention deficit/hyperactivity

disorder, often in combination with hyperactivity and inattention. The effect of the antipsychotics administered is largely mediated by blocking the postsynaptic dopamine D2 receptors. Aripiprazole (a partial D2 receptor antagonist) and risperidone (a D2 receptor antagonist) are the most commonly used antipsychotics and the only medications approved by the US Food and Drug Administration for ASD [74, 75]. Aripripazole is used for ASD to alleviate irritability, hyperactivity, inappropriate language, and stereotypy [76]; risperidone reduces aggression toward others, self-injury, challenging behavior, and rapid mood changes [77]. However, both drugs have significant side effects [75, 78] and it is possible that treatment with MP-10 will eliminate the need for both drugs in patients with FOXP1 syndrome.

Overall, our results strongly suggest that individuals with FOXP1 syndrome may benefit from the administration of MP-10 or other potent PDE10A antagonists, especially if treatment is initiated at a young age. Thus, our study may be the first step towards a specific treatment for FOXP1 syndrome that not only alleviates individual symptoms, but also targets one of the overarching causes of the disorder, namely the imbalance between direct and indirect pathway activity due to reduced levels of Pde10a.

Declarations

Acknowledgment

We acknowledge the expert advice of Dr. Claudia Pitzer and Barbara Kurpiers from the Interdisciplinary Neurobehavioral Core Unit and thank Selina Wunsch for her contribution to the analysis of astrocyte morphology. We acknowledge the technical support of the nCounter Core Facility of Heidelberg University and thank Ralph Röth for support with the performance of the nCounter Sprint and the data analyses. The nCounter Core Facility is partially funded by the CellNetworks Core Technology Platform (CCTP) of Heidelberg University. The CCTP is funded in part by the Federal Ministry of Education and Research (BMBF) and the Ministry of Science Baden-Württemberg within the framework of the Excellence Strategy of the Federal and State Governments of Germany.This work was financially supported by the Deutsche Forschungsgemeinschaft [DFG] Grant FR 3990/3-1. We are grateful to Dr. Rolf Sprengel, Institute for Anatomy and Cell Biology and Max Planck Institute for Medical Research, Heidelberg and Prof. Hannah Monyer, Department of Clinical Neurobiology, Heidelberg, for helpful comments. G.A.R. is a member of the CellNetworks Cluster of Excellence (EXC81), Interdisciplinary Center for Neurosciences, and the Center of Rare Disease.

Author contribution

HF together with GAR planned the experiments. HF supervised and carried out experiments and analyzed results. JW performed the behavioral tests and analyzed the results. NK was involved in the behavioral experiments. FA and TS analyzed microglia and astrocyte morphology with advice from VG. SS helped with transcriptome analysis. CPS supported the study. HF and GAR wrote the paper. All coauthors commented on the paper.

Conflict of interest

The authors declare that they have no conflict of interest.

References

1. Gidziela A, Ahmadzadeh YI, Michelini G, Allegrini AG, Agnew-Blais J, Lau LY *et al.* A meta-analysis of genetic effects associated with neurodevelopmental disorders and co-occurring conditions. *Nat Hum Behav* 2023; **7**(4)**:** 642-656.
2. Meerschaut I, Rochefort D, Revencu N, Petre J, Corsello C, Rouleau GA *et al.* FOXP1-related intellectual disability syndrome: a recognisable entity. *J Med Genet* 2017; **54**(9)**:** 613-623.
3. Rappold G, Siper P, Kostic A, Braden R, Morgan A, Koene S *et al.* FOXP1 Syndrome. In: Adam MP, Feldman J, Mirzaa GM, Pagon RA, Wallace SE, Bean LJH *et al.* (eds). *GeneReviews((R))*: Seattle (WA), 1993.
4. Trelles MP, Levy T, Lerman B, Siper P, Lozano R, Halpern D *et al.* Individuals with FOXP1 syndrome present with a complex neurobehavioral profile with high rates of ADHD, anxiety, repetitive behaviors, and sensory symptoms. *Mol Autism* 2021; **12**(1)**:** 61.
5. Wang J, Frohlich H, Torres FB, Silva RL, Poschet G, Agarwal A *et al.* Mitochondrial dysfunction and oxidative stress contribute to cognitive and motor impairment in FOXP1 syndrome. *Proc Natl Acad Sci U S A* 2022; **119**(8).
6. Wang J, Rappold GA, Frohlich H. Disrupted Mitochondrial Network Drives Deficits of Learning and Memory in a Mouse Model of FOXP1 Haploinsufficiency. *Genes (Basel)* 2022; **13**(1).
7. Frohlich H, Kollmeyer ML, Linz VC, Stuhlinger M, Groneberg D, Reigl A *et al.* Gastrointestinal dysfunction in autism displayed by altered motility and achalasia in Foxp1(+/-) mice. *Proc Natl Acad Sci U S A* 2019; **116**(44)**:** 22237-22245.
8. Niesler B, Rappold GA. Emerging evidence for gene mutations driving both brain and gut dysfunction in autism spectrum disorder. *Mol Psychiatry* 2021; **26**(5)**:** 1442-1444.
9. Kim JH, Hwang J, Jung JH, Lee HJ, Lee DY, Kim SH. Molecular networks of FOXP family: dual biologic functions, interplay with other molecules and clinical implications in cancer progression. *Mol Cancer* 2019; **18**(1)**:** 180.
10. Santos ME, Athanasiadis A, Leitao AB, DuPasquier L, Sucena E. Alternative splicing and gene duplication in the evolution of the FoxP gene subfamily. *Mol Biol Evol* 2011; **28**(1)**:** 237-247.
11. Ferland RJ, Cherry TJ, Preware PO, Morrisey EE, Walsh CA. Characterization of Foxp2 and Foxp1 mRNA and protein in the developing and mature brain. *J Comp Neurol* 2003; **460**(2)**:** 266-279.
12. Hisaoka T, Nakamura Y, Senba E, Morikawa Y. The forkhead transcription factors, Foxp1 and Foxp2, identify different subpopulations of projection neurons in the mouse cerebral cortex. *Neuroscience* 2010; **166**(2)**:** 551-563.
13. Tamura S, Morikawa Y, Iwanishi H, Hisaoka T, Senba E. Foxp1 gene expression in projection neurons of the mouse striatum. *Neuroscience* 2004; **124**(2)**:** 261-267.

14. Anderson AG, Kulkarni A, Harper M, Konopka G. Single-Cell Analysis of Foxp1-Driven Mechanisms Essential for Striatal Development. *Cell Rep* 2020; **30**(9)**:** 3051-3066 e3057.
15. Araujo DJ, Anderson AG, Berto S, Runnels W, Harper M, Ammanuel S *et al.* FoxP1 orchestration of ASD-relevant signaling pathways in the striatum. *Genes Dev* 2015; **29**(20)**:** 2081-2096.
16. Bacon C, Schneider M, Le Magueresse C, Froehlich H, Sticht C, Gluch C *et al.* Brain-specific Foxp1 deletion impairs neuronal development and causes autistic-like behaviour. *Mol Psychiatry* 2015; **20**(5)**:** 632-639.
17. Precious SV, Kelly CM, Reddington AE, Vinh NN, Stickland RC, Pekarik V *et al.* FoxP1 marks medium spiny neurons from precursors to maturity and is required for their differentiation. *Exp Neurol* 2016; **282:** 9-18.
18. Kim DY, Park JS, Leem YH, Park JE, Kim HS. The Potent PDE10A Inhibitor MP-10 (PF-2545920) Suppresses Microglial Activation in LPS-Induced Neuroinflammation and MPTP-Induced Parkinson's Disease Mouse Models. *J Neuroimmune Pharmacol* 2021; **16**(2)**:** 470-482.
19. Lee YY, Park JS, Leem YH, Park JE, Kim DY, Choi YH *et al.* The phosphodiesterase 10 inhibitor papaverine exerts anti-inflammatory and neuroprotective effects via the PKA signaling pathway in neuroinflammation and Parkinson's disease mouse models. *J Neuroinflammation* 2019; **16**(1)**:** 246.
20. Sukhanov I, Dorotenko A, Fesenko Z, Savchenko A, Efimova EV, Mor MS *et al.* Inhibition of PDE10A in a New Rat Model of Severe Dopamine Depletion Suggests New Approach to Non-Dopamine Parkinson's Disease Therapy. *Biomolecules* 2022; **13**(1).
21. Wilson LS, Brandon NJ. Emerging biology of PDE10A. *Curr Pharm Des* 2015; **21**(3)**:** 378-388.
22. Feng X, Ippolito GC, Tian L, Wiehagen K, Oh S, Sambandam A *et al.* Foxp1 is an essential transcriptional regulator for the generation of quiescent naive T cells during thymocyte development. *Blood* 2010; **115**(3)**:** 510-518.
23. Tronche F, Kellendonk C, Kretz O, Gass P, Anlag K, Orban PC *et al.* Disruption of the glucocorticoid receptor gene in the nervous system results in reduced anxiety. *Nat Genet* 1999; **23**(1)**:** 99-103.
24. Wang B, Weidenfeld J, Lu MM, Maika S, Kuziel WA, Morrisey EE *et al.* Foxp1 regulates cardiac outflow tract, endocardial cushion morphogenesis and myocyte proliferation and maturation. *Development* 2004; **131**(18)**:** 4477-4487.
25. Althammer F, Ferreira-Neto HC, Rubaharan M, Roy RK, Patel AA, Murphy A *et al.* Three-dimensional morphometric analysis reveals time-dependent structural changes in microglia and astrocytes in the central amygdala and hypothalamic paraventricular nucleus of heart failure rats. *J Neuroinflammation* 2020; **17**(1)**:** 221.
26. Grauer SM, Pulito VL, Navarra RL, Kelly MP, Kelley C, Graf R *et al.* Phosphodiesterase 10A inhibitor activity in preclinical models of the positive, cognitive, and negative symptoms of schizophrenia. *J Pharmacol Exp Ther* 2009; **331**(2)**:** 574-590.
27. Verhoest PR, Chapin DS, Corman M, Fonseca K, Harms JF, Hou X *et al.* Discovery of a novel class of phosphodiesterase 10A inhibitors and identification of clinical candidate 2-[4-(1-methyl-4-pyridin-4-yl-

1H-pyrazol-3-yl)-phenoxymethyl]-quinoline (PF-2545920) for the treatment of schizophrenia. *J Med Chem* 2009; **52**(16)**:** 5188-5196.

28. Tsai M, Chrones L, Xie J, Gevorkyan H, Macek TA. A phase 1 study of the safety, tolerability, pharmacokinetics, and pharmacodynamics of TAK-063, a selective PDE10A inhibitor. *Psychopharmacology (Berl)* 2016; **233**(21-22)**:** 3787-3795.
29. Escartin C, Galea E, Lakatos A, O'Callaghan JP, Petzold GC, Serrano-Pozo A *et al.* Reactive astrocyte nomenclature, definitions, and future directions. *Nat Neurosci* 2021; **24**(3)**:** 312-325.
30. Petrelli F, Pucci L, Bezzi P. Astrocytes and Microglia and Their Potential Link with Autism Spectrum Disorders. *Front Cell Neurosci* 2016; **10:** 21.
31. Xiong Y, Chen J, Li Y. Microglia and astrocytes underlie neuroinflammation and synaptic susceptibility in autism spectrum disorder. *Front Neurosci* 2023; **17:** 1125428.
32. Seeger TF, Bartlett B, Coskran TM, Culp JS, James LC, Krull DL *et al.* Immunohistochemical localization of PDE10A in the rat brain. *Brain Res* 2003; **985**(2)**:** 113-126.
33. Xie Z, Adamowicz WO, Eldred WD, Jakowski AB, Kleiman RJ, Morton DG *et al.* Cellular and subcellular localization of PDE10A, a striatum-enriched phosphodiesterase. *Neuroscience* 2006; **139**(2)**:** 597-607.
34. Beck G, Maehara S, Chang PL, Papa SM. A Selective Phosphodiesterase 10A Inhibitor Reduces L-Dopa-Induced Dyskinesias in Parkinsonian Monkeys. *Mov Disord* 2018; **33**(5)**:** 805-814.
35. Giampa C, Laurenti D, Anzilotti S, Bernardi G, Menniti FS, Fusco FR. Inhibition of the striatal specific phosphodiesterase PDE10A ameliorates striatal and cortical pathology in R6/2 mouse model of Huntington's disease. *PLoS One* 2010; **5**(10)**:** e13417.
36. Giampa C, Patassini S, Borreca A, Laurenti D, Marullo F, Bernardi G *et al.* Phosphodiesterase 10 inhibition reduces striatal excitotoxicity in the quinolinic acid model of Huntington's disease. *Neurobiol Dis* 2009; **34**(3)**:** 450-456.
37. Kehler J, Nielsen J. PDE10A inhibitors: novel therapeutic drugs for schizophrenia. *Curr Pharm Des* 2011; **17**(2)**:** 137-150.
38. Megens AA, Hendrickx HM, Hens KA, Fonteyn I, Langlois X, Lenaerts I *et al.* Pharmacology of JNJ-42314415, a centrally active phosphodiesterase 10A (PDE10A) inhibitor: a comparison of PDE10A inhibitors with D2 receptor blockers as potential antipsychotic drugs. *J Pharmacol Exp Ther* 2014; **349**(1)**:** 138-154.
39. Nishi A, Kuroiwa M, Miller DB, O'Callaghan JP, Bateup HS, Shuto T *et al.* Distinct roles of PDE4 and PDE10A in the regulation of cAMP/PKA signaling in the striatum. *J Neurosci* 2008; **28**(42)**:** 10460-10471.
40. Suzuki K, Harada A, Suzuki H, Miyamoto M, Kimura H. TAK-063, a PDE10A Inhibitor with Balanced Activation of Direct and Indirect Pathways, Provides Potent Antipsychotic-Like Effects in Multiple Paradigms. *Neuropsychopharmacology* 2016; **41**(9)**:** 2252-2262.
41. Khandelwal N, Cavalier S, Rybalchenko V, Kulkarni A, Anderson AG, Konopka G *et al.* FOXP1 negatively regulates intrinsic excitability in D2 striatal projection neurons by promoting inwardly

rectifying and leak potassium currents. *Mol Psychiatry* 2021; **26**(6)**:** 1761-1774.

42. Kleiman RJ, Kimmel LH, Bove SE, Lanz TA, Harms JF, Romegialli A *et al.* Chronic suppression of phosphodiesterase 10A alters striatal expression of genes responsible for neurotransmitter synthesis, neurotransmission, and signaling pathways implicated in Huntington's disease. *J Pharmacol Exp Ther* 2011; **336**(1)**:** 64-76.
43. Strick CA, James LC, Fox CB, Seeger TF, Menniti FS, Schmidt CJ. Alterations in gene regulation following inhibition of the striatum-enriched phosphodiesterase, PDE10A. *Neuropharmacology* 2010; **58**(2)**:** 444-451.
44. Pettas S, Karagianni K, Kanata E, Chatziefstathiou A, Christoudia N, Xanthopoulos K *et al.* Profiling Microglia through Single-Cell RNA Sequencing over the Course of Development, Aging, and Disease. *Cells* 2022; **11**(15).
45. Harry GJ. Microglia during development and aging. *Pharmacol Ther* 2013; **139**(3)**:** 313-326.
46. Jahn J, Bollensdorf A, Kalischer C, Piecha R, Weiss-Muller J, Potru PS *et al.* Microglial CD74 Expression Is Regulated by TGFbeta Signaling. *Int J Mol Sci* 2022; **23**(18).
47. Potru PS, Spittau B. CD74: a prospective marker for reactive microglia? *Neural Regen Res* 2023; **18**(12)**:** 2673-2674.
48. Leng L, Metz CN, Fang Y, Xu J, Donnelly S, Baugh J *et al.* MIF signal transduction initiated by binding to CD74. *J Exp Med* 2003; **197**(11)**:** 1467-1476.
49. Socodato R, Rodrigues-Santos A, Tedim-Moreira J, Almeida TO, Canedo T, Portugal CC *et al.* RhoA balances microglial reactivity and survival during neuroinflammation. *Cell Death Dis* 2023; **14**(10)**:** 690.
50. Schmidt SI, Blaabjerg M, Freude K, Meyer M. RhoA Signaling in Neurodegenerative Diseases. *Cells* 2022; **11**(9).
51. Choi YR, Kang SJ, Kim JM, Lee SJ, Jou I, Joe EH *et al.* FcgammaRIIB mediates the inhibitory effect of aggregated alpha-synuclein on microglial phagocytosis. *Neurobiol Dis* 2015; **83:** 90-99.
52. Satoh JI, Kino Y, Yanaizu M, Ishida T, Saito Y. Microglia express gamma-interferon-inducible lysosomal thiol reductase in the brains of Alzheimer's disease and Nasu-Hakola disease. *Intractable Rare Dis Res* 2018; **7**(4)**:** 251-257.
53. Ben Achour S, Pascual O. Glia: the many ways to modulate synaptic plasticity. *Neurochem Int* 2010; **57**(4)**:** 440-445.
54. Andoh M, Ikegaya Y, Koyama R. Microglia as possible therapeutic targets for autism spectrum disorders. *Prog Mol Biol Transl Sci* 2019; **167:** 223-245.
55. Andoh M, Ikegaya Y, Koyama R. Synaptic Pruning by Microglia in Epilepsy. *J Clin Med* 2019; **8**(12).
56. Xian H, Watari K, Sanchez-Lopez E, Offenberger J, Onyuru J, Sampath H *et al.* Oxidized DNA fragments exit mitochondria via mPTP- and VDAC-dependent channels to activate NLRP3 inflammasome and interferon signaling. *Immunity* 2022; **55**(8)**:** 1370-1385 e1378.

57. Zhong F, Liang S, Zhong Z. Emerging Role of Mitochondrial DNA as a Major Driver of Inflammation and Disease Progression. *Trends Immunol* 2019; **40**(12)**:** 1120-1133.
58. Alexander GE, DeLong MR, Strick PL. Parallel organization of functionally segregated circuits linking basal ganglia and cortex. *Annu Rev Neurosci* 1986; **9:** 357-381.
59. Gunaydin LA, Kreitzer AC. Cortico-Basal Ganglia Circuit Function in Psychiatric Disease. *Annu Rev Physiol* 2016; **78:** 327-350.
60. Haber SN, Rauch SL. Neurocircuitry: a window into the networks underlying neuropsychiatric disease. *Neuropsychopharmacology* 2010; **35**(1)**:** 1-3.
61. Mencacci NE, Kamsteeg EJ, Nakashima K, R'Bibo L, Lynch DS, Balint B *et al.* De Novo Mutations in PDE10A Cause Childhood-Onset Chorea with Bilateral Striatal Lesions. *Am J Hum Genet* 2016; **98**(4)**:** 763-771.
62. Cheng Y, Wang ZM, Tan W, Wang X, Li Y, Bai B *et al.* Partial loss of psychiatric risk gene Mir137 in mice causes repetitive behavior and impairs sociability and learning via increased Pde10a. *Nat Neurosci* 2018; **21**(12)**:** 1689-1703.
63. Delhaye S, Bardoni B. Role of phosphodiesterases in the pathophysiology of neurodevelopmental disorders. *Mol Psychiatry* 2021; **26**(9)**:** 4570-4582.
64. Layton ME, Kern JC, Hartingh TJ, Shipe WD, Raheem I, Kandebo M *et al.* Discovery of MK-8189, a Highly Potent and Selective PDE10A Inhibitor for the Treatment of Schizophrenia. *J Med Chem* 2023; **66**(2)**:** 1157-1171.
65. Luhach K, Kulkarni GT, Singh VP, Sharma B. Attenuation of neurobehavioural abnormalities by papaverine in prenatal valproic acid rat model of ASD. *Eur J Pharmacol* 2021; **890:** 173663.
66. Schulke JP, Brandon NJ. Current Understanding of PDE10A in the Modulation of Basal Ganglia Circuitry. *Adv Neurobiol* 2017; **17:** 15-43.
67. Louis Sam Titus ASC, Yusuff T, Cassar M, Thomas E, Kretzschmar D, D'Mello SR. Reduced Expression of Foxp1 as a Contributing Factor in Huntington's Disease. *J Neurosci* 2017; **37**(27)**:** 6575-6587.
68. Tang B, Becanovic K, Desplats PA, Spencer B, Hill AM, Connolly C *et al.* Forkhead box protein p1 is a transcriptional repressor of immune signaling in the CNS: implications for transcriptional dysregulation in Huntington disease. *Hum Mol Genet* 2012; **21**(14)**:** 3097-3111.
69. Wilson H, Niccolini F, Haider S, Marques TR, Pagano G, Coello C *et al.* Loss of extra-striatal phosphodiesterase 10A expression in early premanifest Huntington's disease gene carriers. *J Neurol Sci* 2016; **368:** 243-248.
70. Niccolini F, Haider S, Reis Marques T, Muhlert N, Tziortzi AC, Searle GE *et al.* Altered PDE10A expression detectable early before symptomatic onset in Huntington's disease. *Brain* 2015; **138**(Pt 10)**:** 3016-3029.
71. Le Fevre AK, Taylor S, Malek NH, Horn D, Carr CW, Abdul-Rahman OA *et al.* FOXP1 mutations cause intellectual disability and a recognizable phenotype. *Am J Med Genet A* 2013; **161A**(12)**:** 3166-3175.

72. Siper PM, De Rubeis S, Trelles MDP, Durkin A, Di Marino D, Muratet F *et al.* Prospective investigation of FOXP1 syndrome. *Mol Autism* 2017; **8:** 57.
73. Stergachis AB, Neph S, Sandstrom R, Haugen E, Reynolds AP, Zhang M *et al.* Conservation of trans-acting circuitry during mammalian regulatory evolution. *Nature* 2014; **515**(7527)**:** 365-370.
74. Anderson GM, Scahill L, McCracken JT, McDougle CJ, Aman MG, Tierney E *et al.* Effects of short- and long-term risperidone treatment on prolactin levels in children with autism. *Biol Psychiatry* 2007; **61**(4)**:** 545-550.
75. Masi A, DeMayo MM, Glozier N, Guastella AJ. An Overview of Autism Spectrum Disorder, Heterogeneity and Treatment Options. *Neurosci Bull* 2017; **33**(2)**:** 183-193.
76. Hirsch LE, Pringsheim T. Aripiprazole for autism spectrum disorders (ASD). *Cochrane Database Syst Rev* 2016; **2016**(6)**:** CD009043.
77. Jesner OS, Aref-Adib M, Coren E. Risperidone for autism spectrum disorder. *Cochrane Database Syst Rev* 2007; **2007**(1)**:** CD005040.
78. Vazquez-Bourgon J, Ortiz-Garcia de la Foz V, Gomez-Revuelta M, Mayoral-van Son J, Juncal-Ruiz M, Garrido-Torres N *et al.* Aripiprazole and Risperidone Present Comparable Long-Term Metabolic Profiles: Data From a Pragmatic Randomized Controlled Trial in Drug-Naive First-Episode Psychosis. *Int J Neuropsychopharmacol* 2022; **25**(10)**:** 795-806.

Figures

Fig. 1

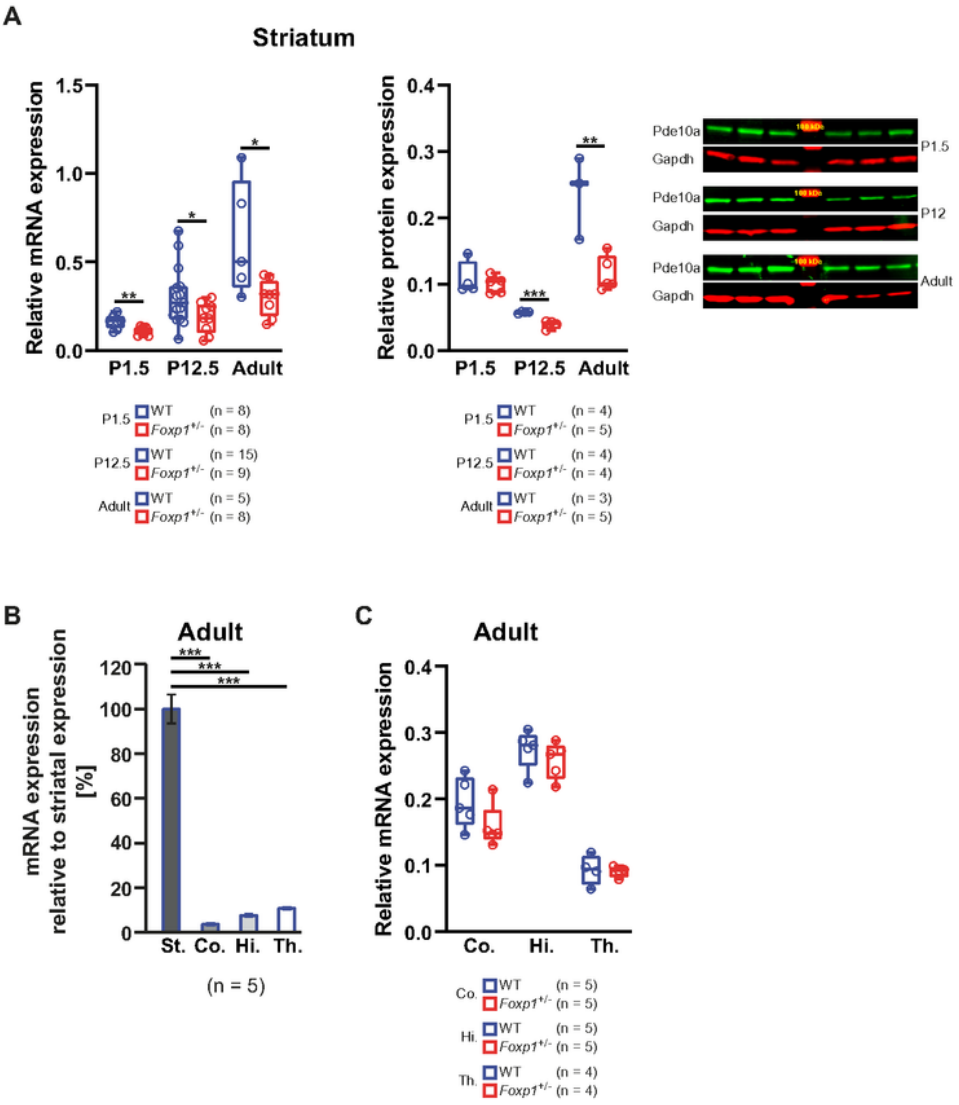

Figure 1

Strong downregulation of Pde10a mRNA and protein in the striatum of *Foxp1*$^{+/-}$ animals from birth until adulthood. A, Relative expression of *Pde10a* mRNA and protein was compared in striatal tissues from WT and *Foxp1*$^{+/-}$ mice at developmental stage P1.5, P12.5 and adulthood by quantitative real-time PCR and Western blot, respectively. **B**, Relative Pde10a mRNA expression in adult cortex (Co.), hippocampus (Hi.), and thalamus (Th.) compared with striatum (St.) quantified by real-time PCR. **C**, Relative Pde10a mRNA

expression in adult WT and *Foxp1*$^{+/-}$ cortex, hippocampus and thalamus quantified by real-time PCR. For the box-and-whisker plot, the boxes represent the first and third quartiles, the whiskers are the 95% confidence interval, and the lines within the boxes are the median. Weak outliers are marked with a circle; asterisks indicate significant difference (**P ≤ 0.01, ***P ≤ 0.001, two-way ANOVA).

Fig. 2

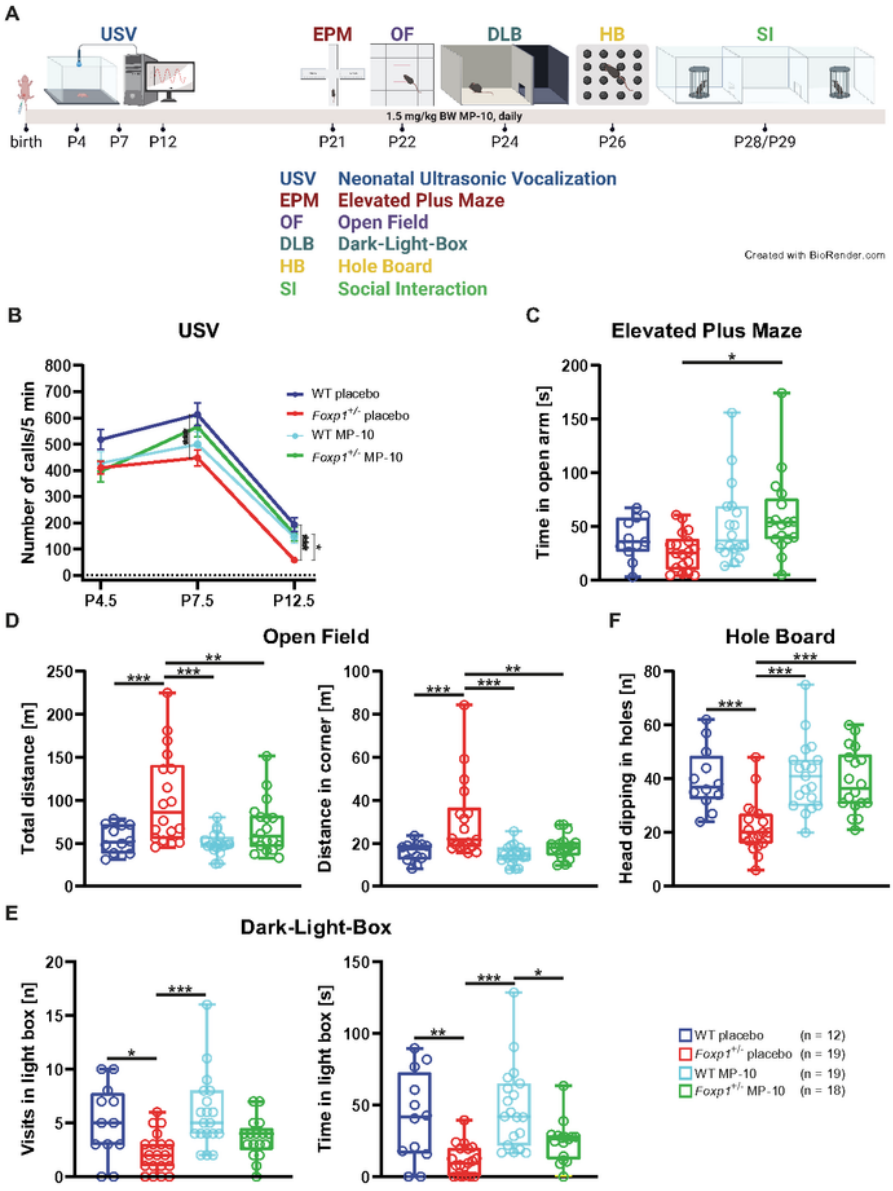

Figure 2

MP-10 is able to reverse behavioral deficits in juvenile *Foxp1*$^{+/-}$ animals. A, Treatment regimen showing the behavioral experiments performed and the respective developmental time point. In all experiments, both placebo-injected and MP-10-treated WT and *Foxp1*$^{+/-}$ mice were examined. **B**, Isolation-induced ultrasonic vocalization (USV) recorded at postnatal days 4.5, 7.5 and 12.5. At all three time points *Foxp1*$^{+/-}$ mice show a reduced number of calls compared to WT animals. MP-10 treated *Foxp1*$^{+/-}$ pups emit a comparable number of ultrasonic calls as WT pups. **C**, Elevated plus maze test; *Foxp1*$^{+/-}$ mice do not show a significant difference in the time spent in the open arms compared to WT animals. However, MP-10 treated *Foxp1*$^{+/-}$ mice, spend significantly more time in the open arms compared to untreated *Foxp1*$^{+/-}$ mice. **D**, Both the total distance traveled and the distance covered in the corner and in the center of the open field are increased compared to WT littermates. *Foxp1*$^{+/-}$ animals treated with MP-10 show no differences in locomotion compared to WT mice. **E**, Dark-light-box test. WT animals enter the light compartment more often than *Foxp1*$^{+/-}$ animals and spend more time there. The number of visits to the light box and the time spent in the light are not different between MP-10 treated *Foxp1*$^{+/-}$ and WT mice. **F**, Hole bord test; WT animals exhibit a significantly higher number of head dipping into the holes than *Foxp1*$^{+/-}$ mice. The number of head dips in MP-10 treated *Foxp1*$^{+/-}$ animals is comparable to WT mice. Placebo-injected WT mice show no significant difference from MP-10-treated WT animals in any of the experiments performed. For the box-and-whisker plot, the boxes represent the first and third quartiles, the whiskers represent the 95% confidence interval, and the lines within the boxes represent the median. Weak outliers are marked with a circle; strong outliers marked with a small grey asterisk were excluded from the statistical calculation. Black asterisks indicate significant difference (*P ≤ 0.05, **P ≤ 0.01, ***P ≤ 0.001, two-way ANOVA followed by Bonferroni post hoc test).

Fig. 3

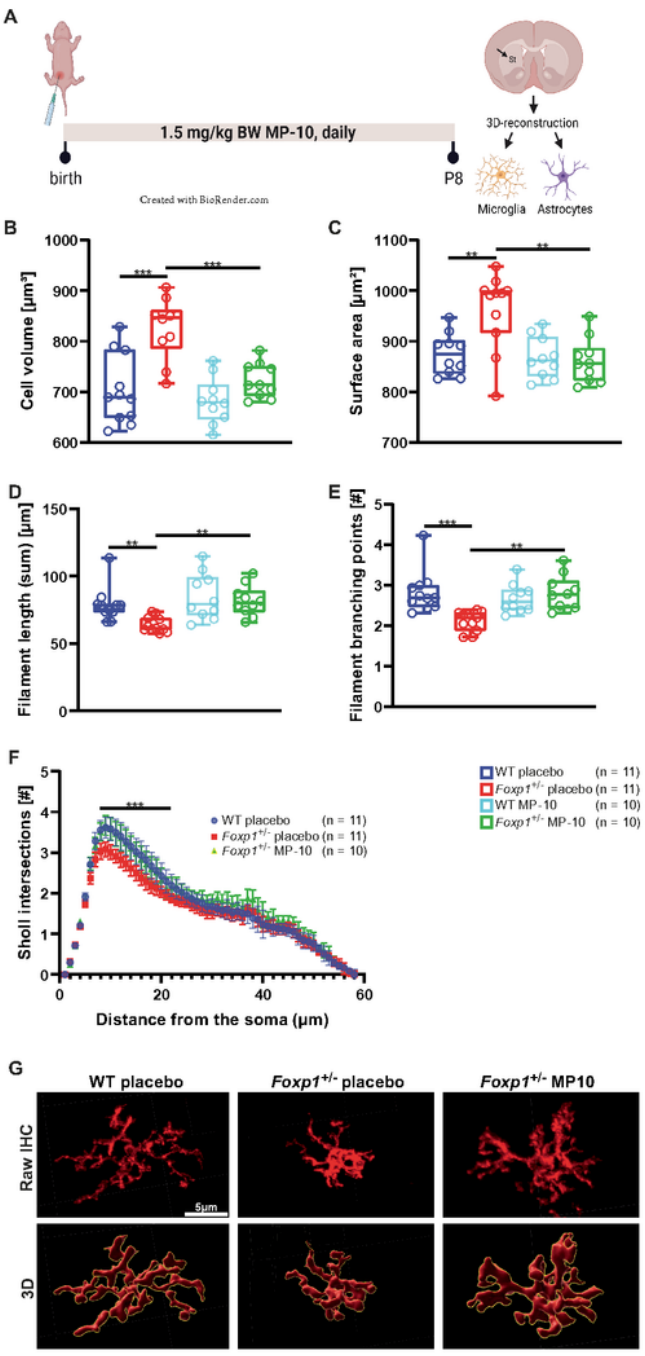

Figure 3

***Foxp1*$^{+/-}$ mice show altered microglial morphology in the striatum at P8, which can be corrected by MP-10 treatment. A**, Treatment scheme; WT and *Foxp1*$^{+/-}$ animals were treated daily with placebo or MP-10, respectively, immediately after birth, and striatal microglia and astrocyte morphology was subsequently assessed by 3D reconstruction with Imaris at P8. Microglia and astrocytes were labeled by immunofluorescent antibody staining for Iba1 and GFAP, respectively. BW, birth weight, St, striatum. **B-F**,

Microglia from placebo-treated *Foxp1*$^{+/-}$ animals show increased cell volume (B) and surface area (C), whereas filament length (D) and filament branching (E, F) are significantly reduced compared to placebo-treated WT animals. MP-10-treated *Foxp1*$^{+/-}$ animals show normal microglial morphology. **G**, Exemplary microglia (green) before (RAW IHC) and after 3D reconstruction (3D) of WT and placebo- or MP-10-treated *Foxp1*$^{+/-}$ tissue. Astrocyte morphology does not differ between the genotypes and is therefore not shown in this figure. For the box-and-whisker plot, the boxes represent the first and third quartiles, the whiskers represent the 95% confidence interval, and the lines within the boxes represent the median. Black asterisks indicate significant difference (**$P \leq 0.01$, ***$P \leq 0.001$, two-sided t-test).

Fig. 4

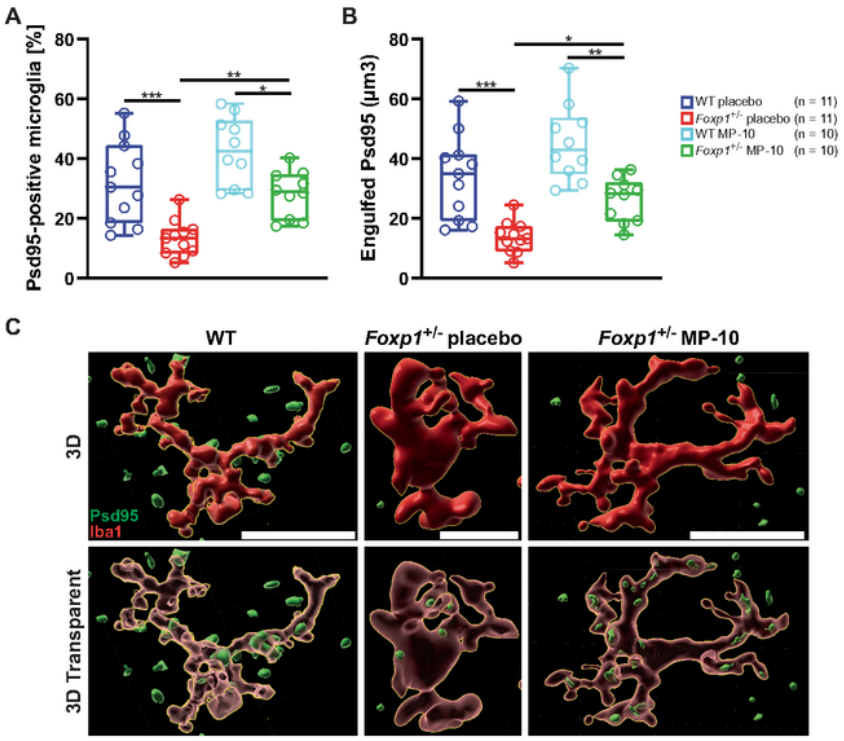

Figure 4

Synaptic pruning is significantly increased in the striatum of untreated *Foxp1*$^{+/-}$ mice at P8, but not in MP-10-treated *Foxp1*$^{+/-}$ animals. To examine synaptic pruning in those mice that were treated daily with placebo or MP-10 immediately from birth to P8, microglia and synapses were labeled by fluorescent antibody staining for Iba1(red) and Psd95 (green), respectively. **A**, **B**, Both the number of synapse engulfing microglia and the amount of engulfed synaptic material are significantly increased in *Foxp1*$^{+/-}$

striata. *Foxp1*$^{+/-}$ animals treated with MP-10 show no differences in synaptic pruning compared to WT animals. **C**, Exemplary microglia (green) with synapse (red) before (RAW IHC) and after 3D reconstruction (3D) of WT and placebo or MP-10 treated *Foxp1*$^{+/-}$ tissue. For the box-and-whisker plot, the boxes represent the first and third quartiles, the whiskers represent the 95% confidence interval, and the lines within the boxes represent the median. Black asterisks indicate significant difference (*P ≤ 0.05, **P ≤ 0.01, ***P ≤ 0.001, two-sided t-test (A-E) and two-way ANOVA (F).

Fig. 5

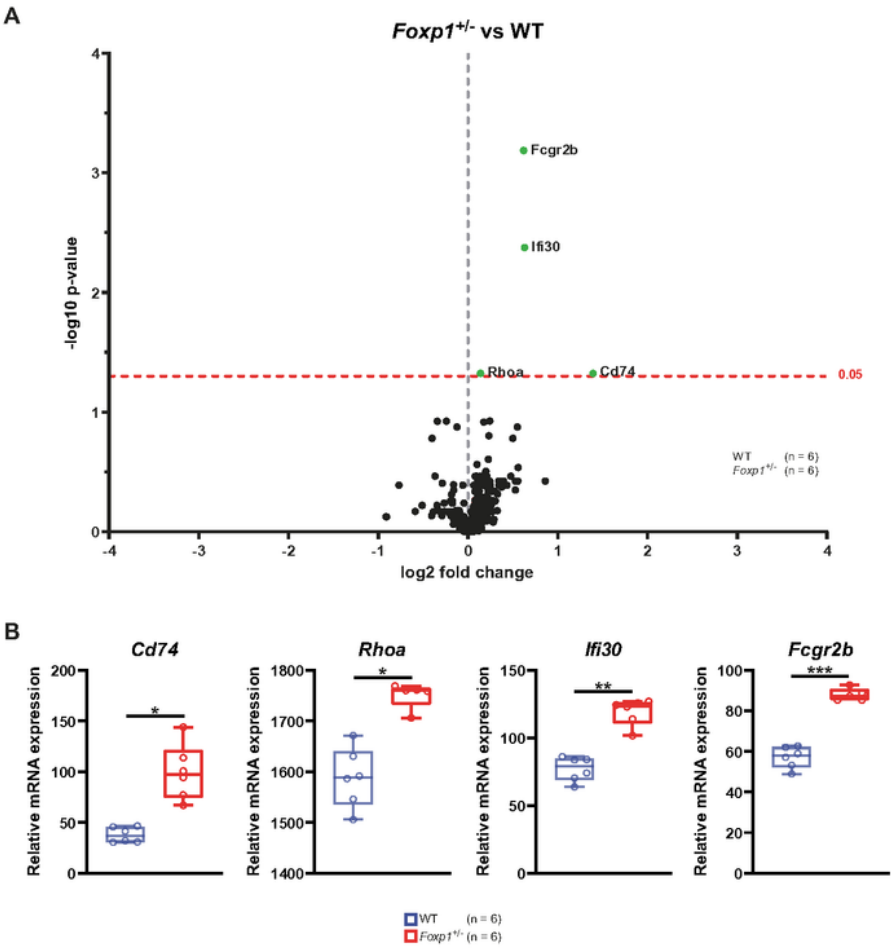

Figure 5

Expression of neuroinflammatory marker genes in the *Foxp1*$^{+/-}$ striatum at P8. To investigate the extent to which there is evidence of neuroinflammation in *Foxp1*$^{+/-}$ striatal tissue, an nCounter analysis was performed containing a neuroinflammation panel including 770 targets. **A**, Volcano plot of differential gene expression between *Foxp1*$^{+/-}$ and WT. The labeled genes are those that show a significant change in expression. **B**, Relative mRNA expression of the four genes significantly altered in *Foxp1*$^{+/-}$ tissue (*Cd74*, *Rhoa*, *Ifi30* and *Fcgr2b*) in WT and *Foxp1*$^{+/-}$ pups. For the box-and-whisker plot, the boxes represent the first and third quartiles, the whiskers represent the 95% confidence interval, and the lines within the boxes represent the median. Black asterisks indicate significant difference (*P ≤ 0.05, **P ≤ 0.01, ***P ≤ 0.001).

Supplementary Files

This is a list of supplementary files associated with this preprint. Click to download.

- Suppl.Fig.1.pdf
- Suppl.Fig.2.pdf
- Table1.pdf
- Table2.xlsx